Electronic Supplementary Material (ESI) for ChemComm.

Supporting Information

An All-Inorganic Polyoxometalate-Polyoxocation Chemical Garden

Laurie J. Points,[†] Geoffrey J. T. Cooper,[†] Pierre Mialane,[‡] and Leroy Cronin[†]*

[†]WestCHEM, School of Chemistry, University of Glasgow, University Avenue, Glasgow, G12 8QQ, United Kingdom

[‡]Institut Lavoisier de Versailles, UMR 8180, Université de Versailles Saint-Quentin en Yvelines, 45 Avenue des Etats-Unis, 78035 Versailles cedex, France

Table of Contents

1. Supporting videos
2. POM structures
3. Experimental and instrumental details
4. Data and plots
5. Optical microscopy images
6. SEM images

1. Supporting Videos

Supporting Video SV1 – An example of the precipitation clouds observed at low concentrations (here 0.5 mM), which eventually form a large membrane. Sped up by a factor of 5.

Supporting Video SV2 – An example of the cloud and membrane observed at 1 mM **2** when the membrane does not burst to form a tube. Sped up by a factor of 10.

Supporting Video SV3 – The membranes and tubes growth regime observed at 1 mM **2**. Sped up by a factor of 30.

Supporting Video SV4 – The slugs growth regime observed at 2 mM **2**. Sped up by a factor of 30.

Supporting Video SV5 – The tubes and slugs observed at 5 mM **2**. Sped up by a factor of 30.

Supporting Video SV6 – The tubes and jetting observed at 10 mM **2**. Sped up by a factor of 30.

Supporting Video SV7 – The jetting and budding growth regimes observed at 20 mM. **2**. Sped up by a factor of 10.

Supporting Video SV8 – Microcrystallite growth and precipitation observed at 5 mM **2**. Sped up by a factor of 10.

2. POM Structures

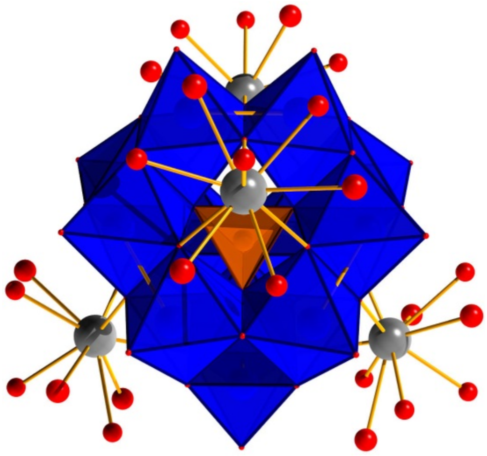

Figure S 1 – Polyhedral representation, in which the colour of the polyhedra represents the central metal atom, of the Structure of 1 - $[\varepsilon\text{-}PMo_{12}O_{36}(OH)_4\{La(H_2O)_{2.5}\}_4]^{5+}$. Blue – Mo, Orange – P, Grey – La, Red – O.

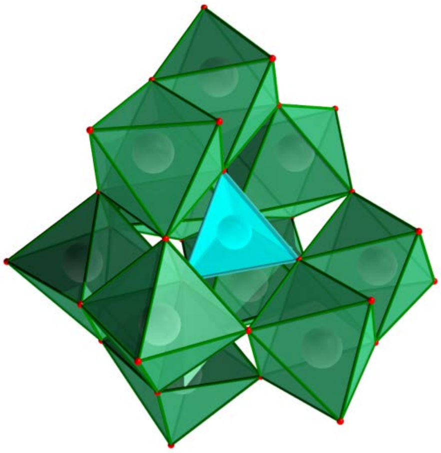

Figure S 2 – Polyhedral representation, in which the colour of the polyhedra represents the central metal atom, of the structure of 2 - $[\gamma\text{-}SiW_{10}O_{36}]^{8-}$. Red – O, Green – W, Teal – Si.

3. Experimental and Instrumental Details

Instrumentation

Optical Microscopy

Colour optical microscopy has been performed using an Olympus IX-81 inverted microscope with a mounted with a Mikrotron GmbH EoSense CL color (MC1363) camera. All image analysis was conducted using Media Cybernetics Image-Pro Premier Version 9.0.4. The images used to generate data for Figures 3 and 4 were taken using Keyence VHX 600 digital microscope with a mounted VHZ 20R objective.

SEM

SEM was performed on a Hitachi S-4700 SEM instrument using acceleration voltages of 10-20 kV. Samples were Au/Pd sputter coated using a Poloron SC7640 sputter coater.

FAAS/FAES

FAAS/FAES was performed at the Environmental Chemistry Section, School of Chemistry, University of Glasgow on a Perkin Elmer AA400 atomic absorption spectrometer.

POM Synthetic Procedures

Potassium γ-Decatungstosilicate, $K_8[\gamma\text{-}SiW_{10}O_{36}].12H_2O$ (2)

Potassium γ-Decatungstosilicate **(2)** is prepared as per the reported literature procedure, which is repeated here for completeness.[1] **2** is prepared from potassium β_2-undecatungstosilicate, $K_8[\beta_2\text{-}SiW_{11}O_{39}].14H_20$, which is prepared as follows:

Sodium metasilicate (11 g, 50 mmol) is dissolved in 100 mL of water (Solution A). Sodium tungstate (182 g, 0.55 mol) is dissolved in 300 mL of water in a separate 1 L beaker containing a magnetic stirrer bar. To this solution, 165 mL of 4M HCl is added in 1 mL portions over 10 min, with vigorous stirring (there is a local formation of hydrated tungstic acid that slowly disappears). Then, Solution A is poured into the tungstate solution, and the pH is adjusted to between 5 and 6 by addition of the 4 M HCl solution (~40 mL). This pH is maintained by addition of small amounts of 4 M HCl for 100 minutes. Solid potassium chloride (90 g) is then added to the solution with gentle stirring. After 15 min, the precipitate is collected by filtering through a sintered glass filter. Purification is achieved by dissolving the product in 850 mL of water. The insoluble material is rapidly removed by filtration on a fine frit, and the salt is precipitated again by addition of solid KCl (80 g). The precipitate is separated by filtration, washed with 2 M potassium chloride solution (2 portions of 50 mL), and air dried.

Potassium β_2-undecatungstosilicate (15 g, 5 mmol), synthesized as above, is dissolved in 150 mL of water maintained at room temperature. Impurities in the $K_8[\beta_2\text{-}SiW_{11}O_{39}]$ salt (mainly paratungstate) give insoluble materials, which have to be removed rapidly by filtration on a fine frit or through Celite. The pH of the solution is quickly adjusted to 9.1 by addition of a 2 M aqueous solution of K_2C0_3. The pH of the solution is kept at this value by addition of the K_2CO_3 solution for exactly 16 min. The potassium salt of the γ-decatungstosilicate is then precipitated by addition of solid potassium chloride (40 g). During the precipitation (10 min), the pH must be maintained at 9.1 by addition of small amounts of the K_2CO_3 solution. The solid is removed by filtering, washed with 1 M KCl solution, and air dried. Yield: c. 10 g (70 %). Reaction success verified by CHN elemental analysis and FTIR spectroscopy by comparison to literature values.[1]

$[\varepsilon\text{-}PMo_{12}O_{36}(OH)_4\{La(H_2O)_{2.5}Cl_{1.25}\}_4]\cdot 27H_2O_{(s)}$ (1)

$[\varepsilon\text{-}PMo_{12}O_{36}(OH)_4\{La(H_2O)_{2.5}Cl_{1.25}\}_4]\cdot 27H_2O_{(s)}$ is sourced from the Mialane group at The University of Versailles, where it is prepared as reported in the literature.[2]

Typical Tube Growth Experiment

In a typical tube growth experiment, a few crystals of **1** were placed on a microscope slide using a needle. Whilst observing using optical microscopy 0.2 - 0.5 mL of **2** was carefully added to the microscope slide, to initiate the osmotic pump system. A micromanipulator was often used to pin the crystal in place, to prevent the crystals washing to the side of the droplet on addition of **2**. Still images, time lapse experiments and videos were recorded.

Aqueous Solubility Determination

To determine the aqueous solubility of **2** 10 mL of saturated aqueous solution of **2** was prepared. Excess insoluble material was then filtered off, and the sample left to dry in ambient conditions, then in a desiccator. The weight gain of the vial was then used to calculate the solubility. This was done in triplicate and the results are shown in Table S 1

Table S 1 – The results for the aqueous solubility determination of 2.

Weight Gain / g	Solubility / mgmL^{-1}
1.5088	150.88
1.5073	150.73
1.4948	149.48
Average	150.37

This is equivalent to c. 50.6 mM.

4. Data and Plots

All image analysis was conducted using Media Cybernetics Image-Pro Premier Version 9.0.4.

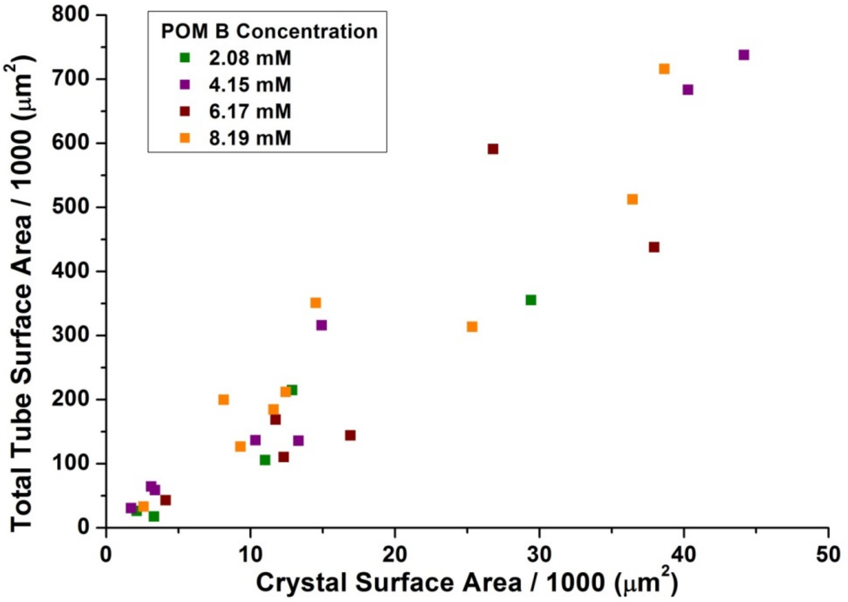

Figure S 3 - A plot showing the linear correlation between the crystal surface area and the tube surface area formed, when measured from above. This is the same plot as Figure 3.

Data processing – Optical images for this data were acquired using a Keyence VHX 600 digital microscope with a mounted VHZ 20R objective. Images were taken every 15 s after the addition of a solution of **2**. After calibration, the 'Auto Trace Polygon' feature was used to measure the crystal and tube surface areas, as measured from above. These were measured in the first image and in the first image in which the tube no longer grew, with manual correction when the auto trace feature strayed from the correct boundary.

Data:

Crystal Surface Area /	Total Tube Surface Area /	Concentration

1000	**1000**	
µm^2	**µm^2**	**mM**
29.41	355.22	2.08
11.01	105.67	2.08
3.32	17.36	2.08
12.87	214.55	2.08
2.10	26.32	2.08
3.37	58.68	4.15
3.12	64.42	4.15
1.73	30.50	4.15
14.92	315.78	4.15
10.34	136.55	4.15
13.30	135.71	4.15
44.16	738.00	4.15
40.28	683.39	4.15
4.12	42.94	6.17
11.73	168.67	6.17
12.29	110.45	6.17
37.94	438.03	6.17
16.90	144.15	6.17
26.79	591.14	6.17
38.65	716.14	8.19
14.51	351.00	8.19
2.59	33.05	8.19
8.14	199.56	8.19
12.43	212.00	8.19
25.35	313.63	8.19
9.29	126.54	8.19
36.45	512.48	8.19
11.59	184.71	8.19

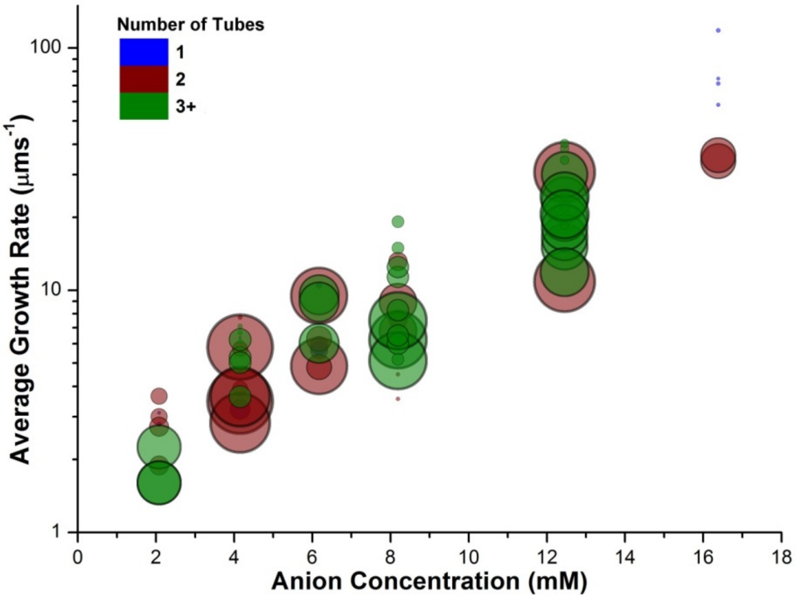

Figure S 4 - A plot showing the exponential trend between the anion (2) concentration and the tube growth rate. The size of the bubble is proportional to the visible crystal surface area. This is the same data as for Figure 4, except with crystal size also plotted as bubble surface area.

Data processing – Optical images for this data were acquired using a Keyence VHX 600 digital microscope with a mounted VHZ 20R objective. Images were taken every 15 s after the addition of a solution of **2**. The average growth rate was found by measuring the size of the tube at its greatest extent (using the 'Auto Trace Polygon' feature with manual correction) and dividing by the time it took for this tube to form. For the measure of 'number of tubes', only structures resembling the slugs and tubes growth regimes were counted due to the fact that structures in the jetting and budding regimes could not accurately be measured due to their thin and three-dimensional nature. The crystal surface area was measured using the 'Auto Trace Polygon' for the first image with manual correction when the auto trace feature strayed from the correct boundary.

Data:

Anion Concentration	**Average Growth Rate**	**Crystal Surface Area / 1000**	**Number of Tubes**
mM	**μms^{-1}**	**μm^2**	
2.08	2.79	3.32	1
2.08	3.11	2.1	1
4.15	6.38	1.73	1
4.15	3.22	13.3	1
6.17	10.48	4.12	1
6.17	5.65	11.73	1
6.17	5.92	12.29	1
16.38	118.15	3	1
16.38	58.27	2.44	1
16.38	74.78	2.36	1
16.38	71.29	2.89	1

Anion Concentration	**Average Growth Rate**	**Crystal Surface Area / 1000**	**Number of Tubes**

mM	µms^{-1}	µm^{2}	
2.08	3	11.01	2
2.08	3.65	11.01	2
2.08	1.89	12.87	2
2.08	2.73	12.87	2
4.15	4.66	3.12	2
4.15	7.73	3.12	2
4.15	5.71	10.34	2
4.15	3.92	10.34	2
4.15	3.48	44.16	2
4.15	5.82	44.16	2
4.15	2.83	40.28	2
4.15	3.63	40.28	2
6.17	9.48	37.94	2
6.17	4.86	37.94	2
6.17	4.81	16.9	2
6.17	6.29	16.9	2
8.19	3.56	2.59	2
8.19	4.49	2.59	2
8.19	7.55	12.43	2
8.19	13.13	12.43	2
8.19	6.79	25.35	2
8.19	8.92	25.35	2
12.45	10.85	40.95	2
12.45	30.67	40.95	2
16.38	34.14	23.51	2
16.38	36.08	23.51	2

Anion Concentration	**Average Growth Rate**	**Crystal Surface Area / 1000**	**Number of Tubes**
mM	**µms^{-1}**	**µm^{2}**	
2.08	1.6	29.41	3
2.08	2.25	29.41	3
2.08	1.6	29.41	3
4.15	6.14	3.37	3
4.15	6.67	3.37	3
4.15	7.09	3.37	3
4.15	5.26	14.92	4
4.15	3.63	14.92	4
4.15	5.02	14.92	4
4.15	6.25	14.92	4
6.17	9.57	26.79	3
6.17	6.03	26.79	3
6.17	8.93	26.79	3
8.19	6.24	38.65	3
8.19	5.12	38.65	3
8.19	7.48	38.65	3
8.19	8.27	14.51	5
8.19	6.01	14.51	5

8.19	11.34	14.51	5
8.19	6.5	14.51	5
8.19	12.45	14.51	5
8.19	5.18	8.14	3
8.19	19.17	8.14	3
8.19	14.93	8.14	3
12.45	15.1	30.85	6
12.45	23.58	30.85	6
12.45	16.5	30.85	6
12.45	19.83	30.85	6
12.45	30.01	30.85	6
12.45	18.16	30.85	6
12.45	24.22	5.71	6
12.45	38.53	5.71	6
12.45	40.39	5.71	6
12.45	21.77	5.71	6
12.45	34.41	5.71	6
12.45	18.47	5.71	6
12.45	11.87	32.52	3
12.45	24.43	32.52	3
12.45	20.6	32.52	3

FAAS/FAES Elemental Analysis Results

Batch tube growth experiments were used to prepare samples for FAAS/FAES elemental analysis. Similar to a normal tube growth experiment, a needle was used to place a number of crystals on a slide. To this was added 400 µL of **2** solution to initiate precipitate formation. After 5 minutes the supernatant was removed and filtered to remove any suspended precipitate. This was repeated 12 times for each sample. The solutions were then brought to a concentration of 0.1 % KCl, to control ionisation, by addition of an appropriate amount of 1.0 % KCl solution. A further 1:5 dilution in water was also used in some cases to bring the La concentration within the linear range.

Mo : La ratio by mass 2.07 : 1.00 (i.e. expected Mo : La ratio if they leech into the supernatant at the same rate.)

Concentration 2	**Mo Concentration**	**La Concentration**	**Mo:La Ratio**
mM	**mgmL^{-1}**	**mgmL^{-1}**	
1	4.16	26.1	0.16 : 1
5	4.55	113.3	0.04 : 1
20	13.2	143.6	0.09 : 1
Mean			0.10 : 1

As can be seen from the above table, significantly more La has leeched into the supernatant than Mo, especially considering the higher mass content of Mo in **1**.

5. Optical Microscopy Images

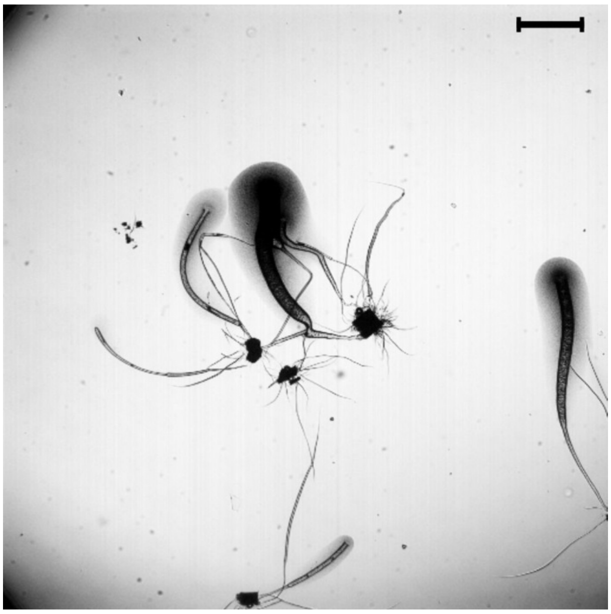

Figure S 5 – An optical microscopy image showing the growth plumes around growing tubes. This image is of tube growth from 10 mM 2. Scale bar = 400 µm.

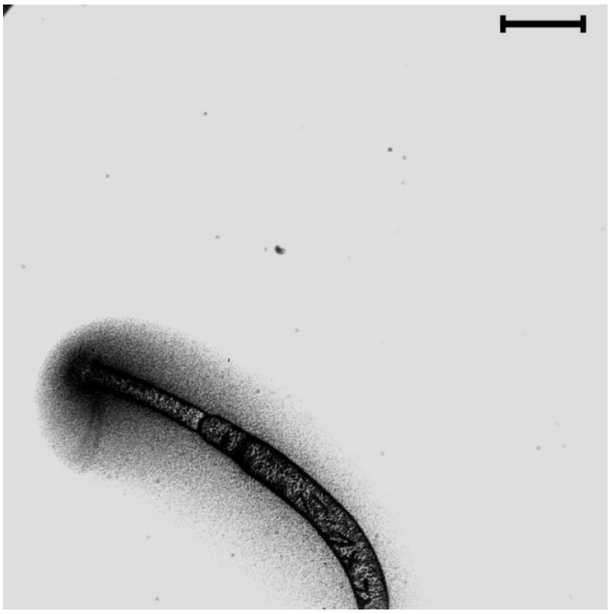

Figure S 6 - An optical microscopy image showing a growth plume around a growing tube as well as the microcrystallites growing within the tube. Some rising material can also be seen at the tube head. This image is of tube growth from 10 mM 2. Scale bar = 200 µm.

Diameter Changes

Both step and gradual diameter changes have been observed in this POM chemical garden system, as illustrated in figure S7. These are most likely to be due to initiation, termination and merging events in other tubes growing simultaneously from the same crystal. In the charge-normal systems only one tube is typically observed, hence these events could not occur, although these diameter effects could also point to more complex mechanisms and processes occurring in this system.

Diameter changes can also be induced by changing the anion concentration during a tube growth experiment, as shown in Figure S7. Initially, when the second solution is added, the growth cloud is washed away and tube growth stops, due to a lack of cations. This may cause the tube to seal and tube growth to terminate completely, the tube to seal and then a smaller tube to initiate some time later or the tube may not seal, and the smaller tube initiates straight away (as was observed in Figure S7).

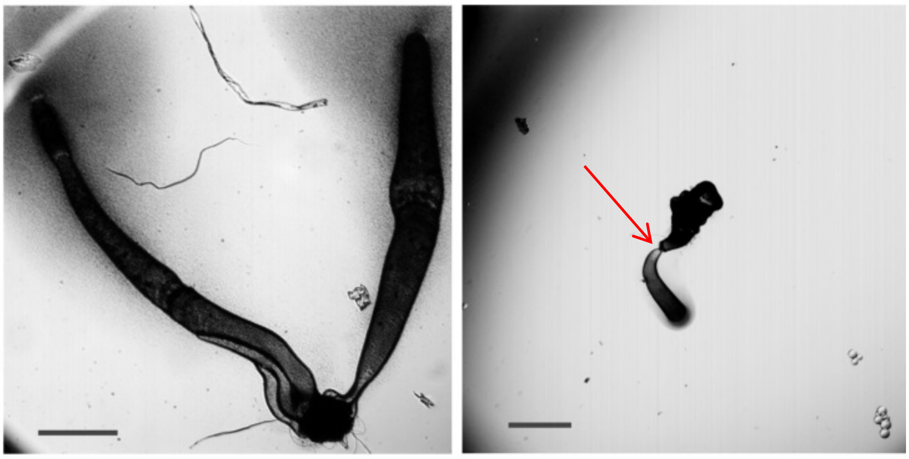

Figure S 7 - Optical microscopy images of the diameter changes that occur during tube growth (left,) and on the addition of a more concentrated anion solution to a growing tube (right, B). In this case, a tube is already growing in 200 µL of 2 mM 2, to which 50 µL of 14 mM 2 is added, giving a final concentration of 4.4 mM. The point at which the more concentrated solution was added is indicated by the red arrow. Scale bars 200 µm (left), 400 µm (right).

Unmodified Images Used For Figure 2

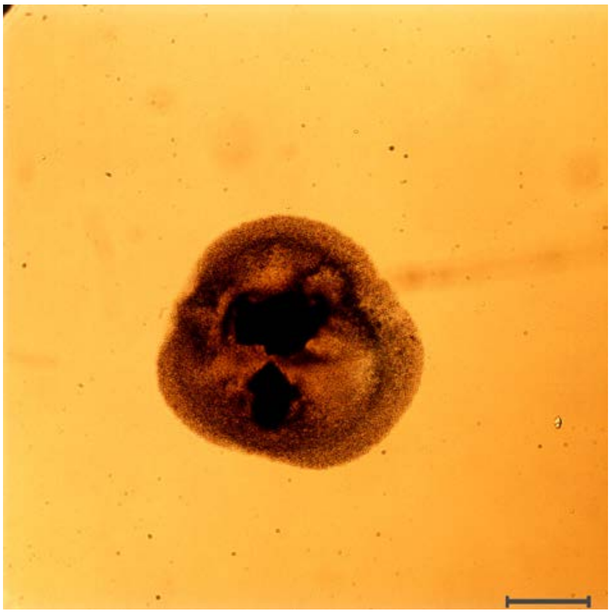

Figure S 8 - The image used for ≤1 mM clouds lower. Scale bar is 200 µm and this image was taken 30 seconds after the anion solution was added.

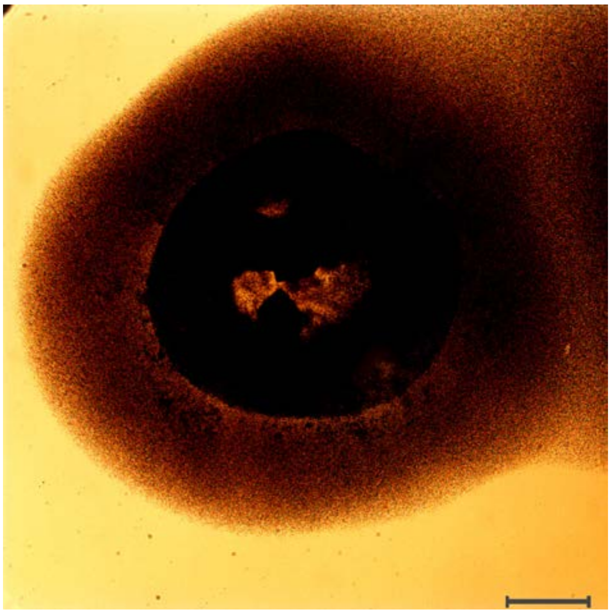

Figure S 9 - The image used for ≤1 mM clouds upper. Scale bar is 200 µm and this image was taken 4 minutes after the anion solution was added.

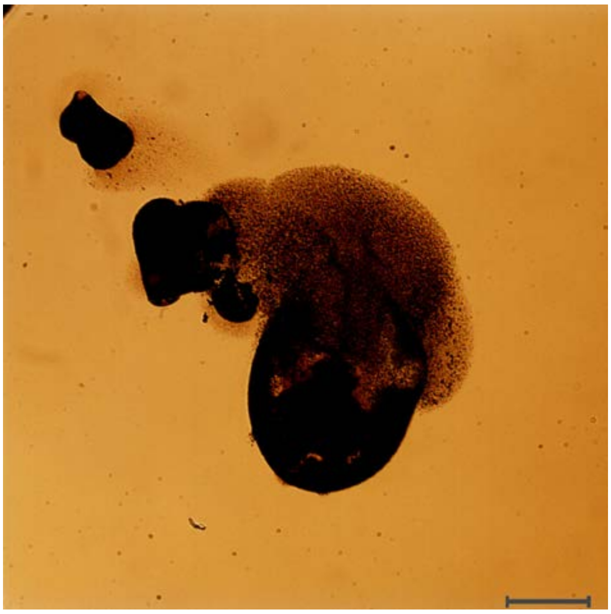

Figure S 10- The image used for 1 mM membranes and tubes lower. Scale bar is 200 µm and this image was taken a minute after the anion solution was added.

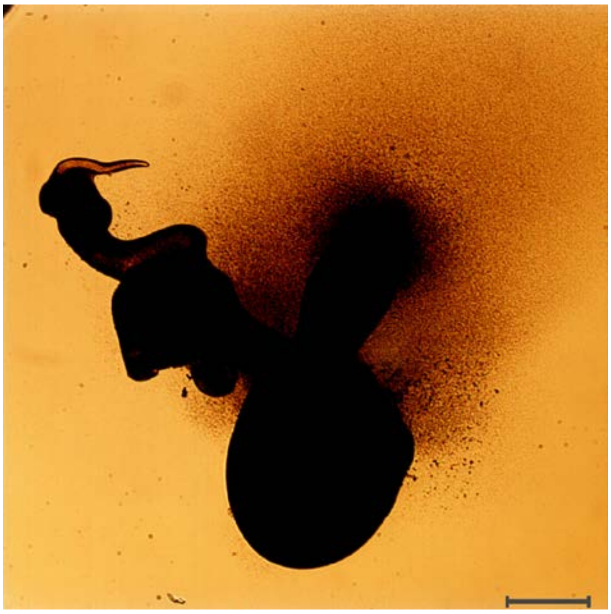

Figure S 11 - The image used for 1 mM membranes and tubes upper. Scale bar is 200 µm and this image was taken 14 minutes and 20 seconds after the anion solution was added.

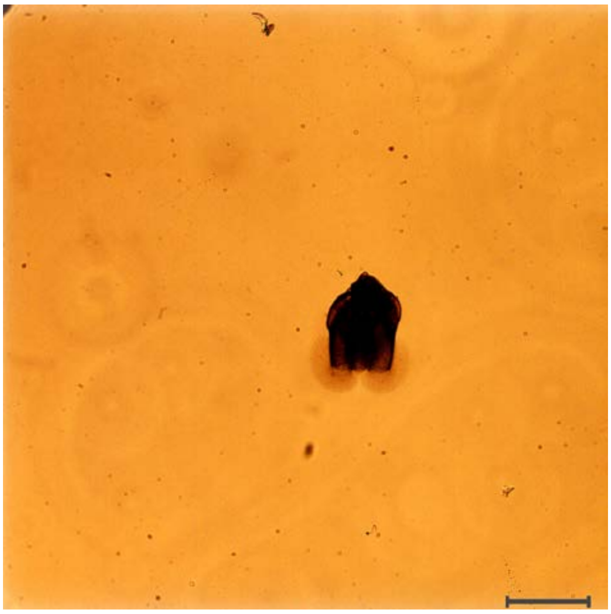

Figure S 12 - The image used for 2 mM slugs lower. Scale bar is 200 µm and this image was taken 45 seconds after the anion solution was added.

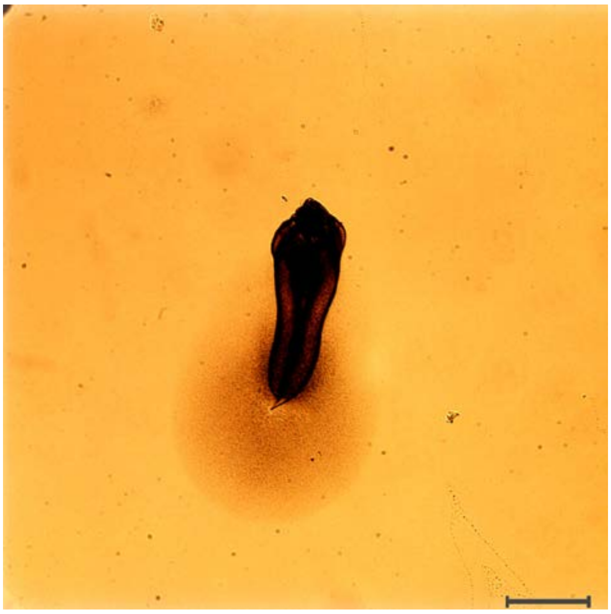

Figure S 13 - The image used for 2 mM slugs upper. Scale bar is 200 µm and this image was taken 3 minutes after the anion solution was added.

Figure S 14 - The image used for 5 mM upper. Scale bar is 400 µm and this image was taken 1 minute after the anion solution was added.

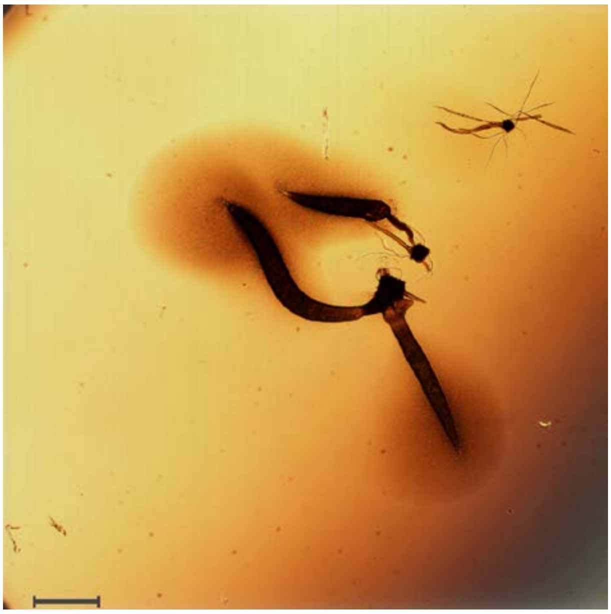

Figure S 15 - The image used for 5 mM upper. Scale bar is 400 µm and this image was taken 4 minutes and 20 seconds minute after the anion solution was added.

Figure S 16 - The image used for 10 mM lower. Scale bar is 400 µm and this image was taken 30 seconds after the anion solution was added.

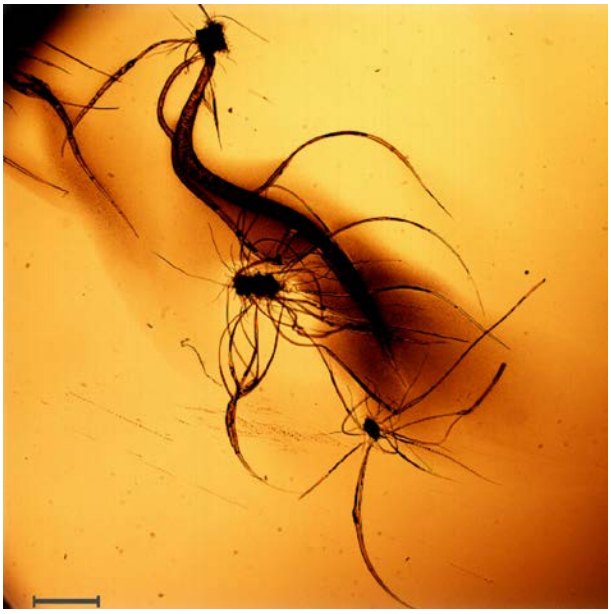

Figure S 17 - The image used for 10 mM upper. Scale bar is 400 µm and this image was taken 5 minutes and 30 seconds after the anion solution was added.

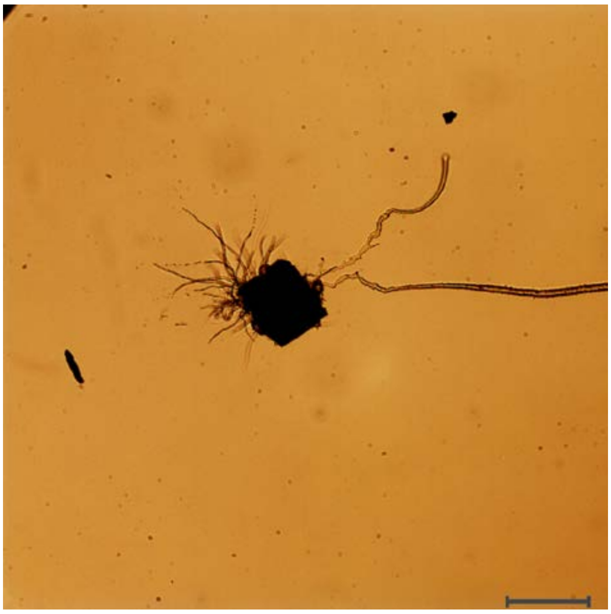

Figure S 18 - The image used for 20 mM lower. Scale bar is 200 µm and this image was taken 30 seconds after the anion solution was added.

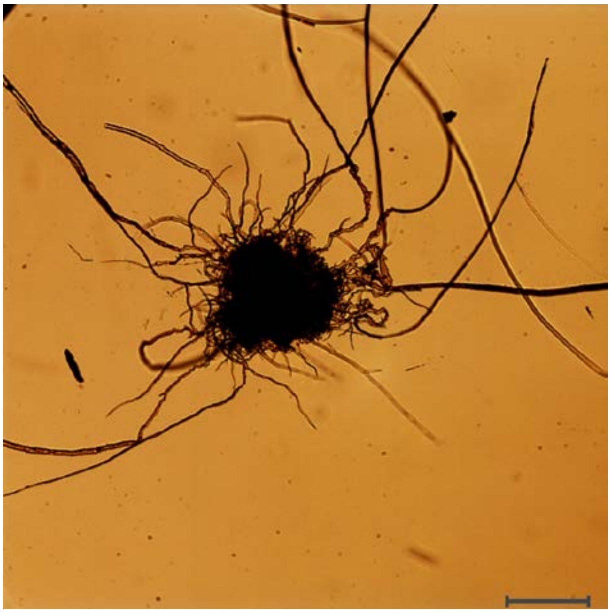

Figure S 19 - The image used for 20 mM lower. Scale bar is 200 µm and this image was taken 5 minutes and 30 seconds after the anion solution was added.

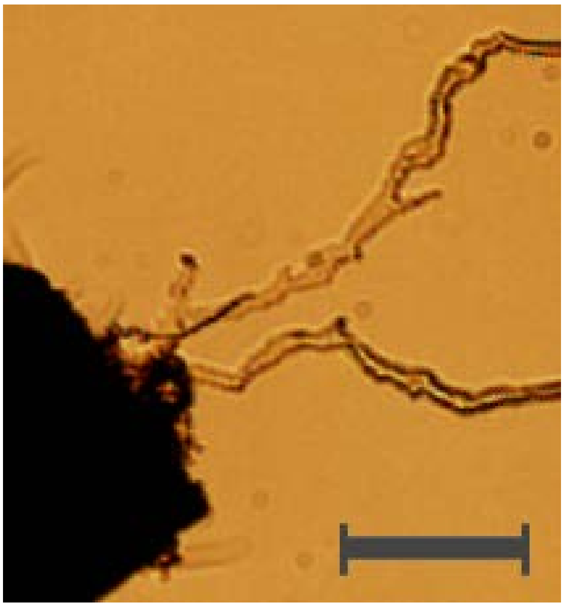

Figure S 20 – A close up of one area of Figure S 18 showing the structure formed by the budding growth regime. Scale bar 100 µm.

6. SEM Images

A selection of SEM images from each concentration are shown here. All cracks and damage are thought to occur during sample washing and preparation. To prepare the SEM samples, **2** is added to **1** using the normal experimental procedure. After this, the sample is carefully rinsed with deionised water and allowed to dry under ambient conditions. For SEM sample preparation the sample is coated for 60 s with Au/Pd alloy using a Poloron SC7640 sputter coater.

1 mM

These images show a pair of crystals which have formed a three dimensional semi-permeable membrane which has then burst to form a short tube. There is also a short tube which has grown from the end of a larger tube after the initial larger tube has terminated. These SEM images are for the sample shown in supporting video SV3.

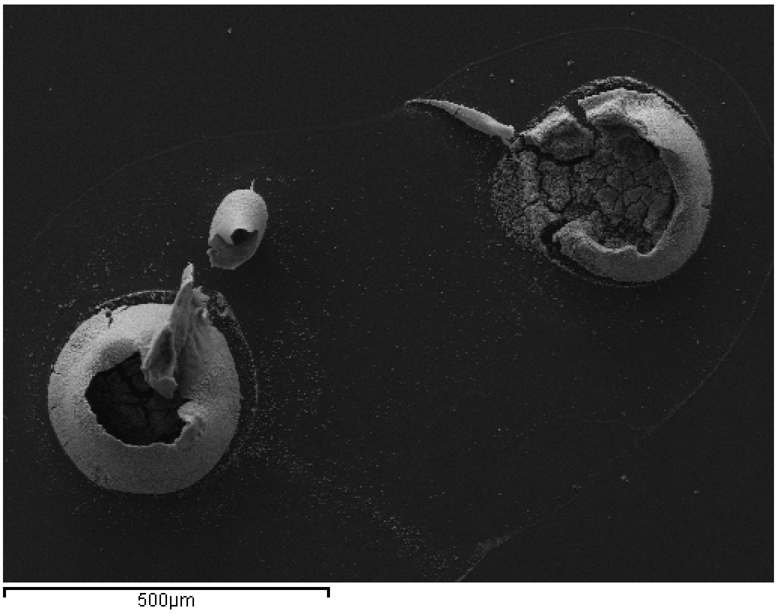

Figure S 21 – SEM images of the precipitation structures formed around two crystals on addition of 1 mM 2.

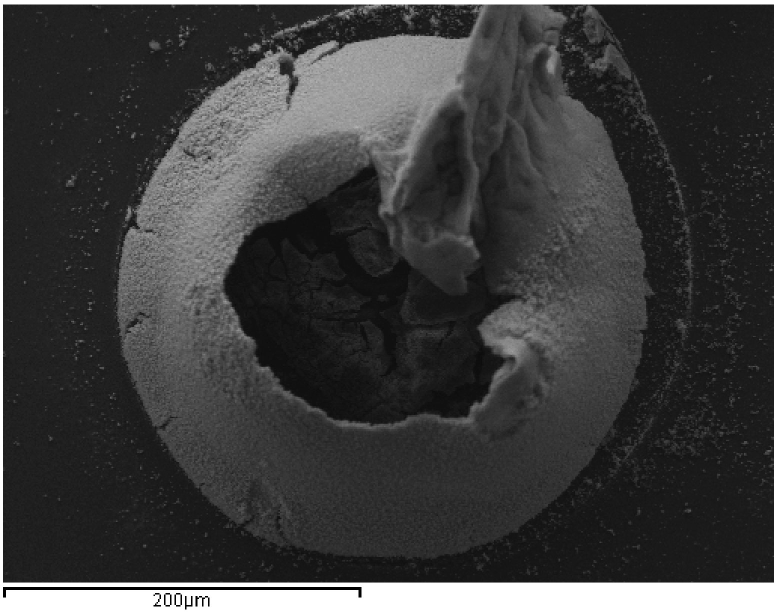

Figure S 22 – Higher magnification SEM image of one of the membranes.

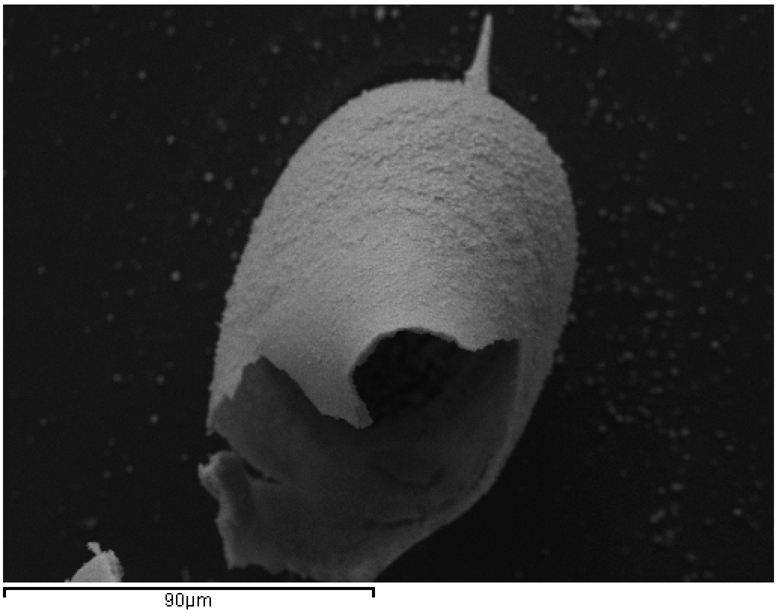

Figure S 23 – SEM image of a broken off tube, showing its low aspect ratio and the short tube that initiated after the initial tube had terminated.

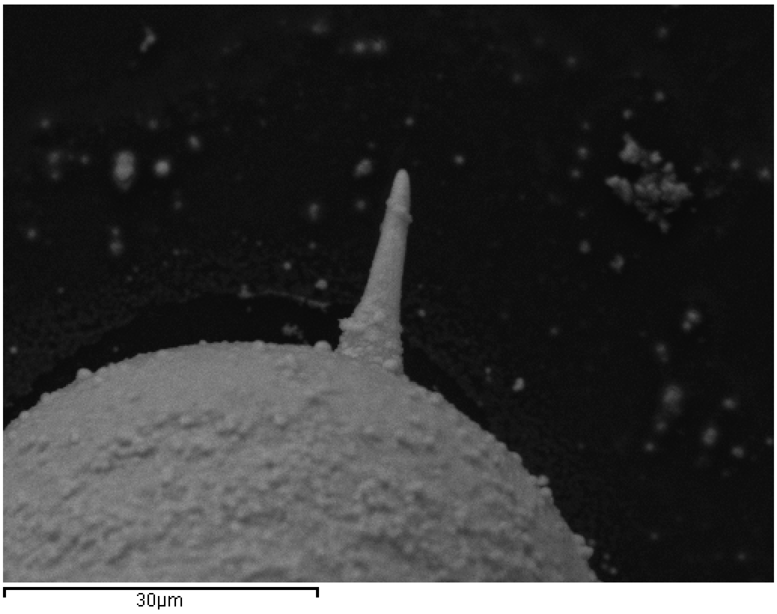

Figure S 24 – Higher magnification SEM image of the second, smaller tube that initiated after the larger tube terminated.

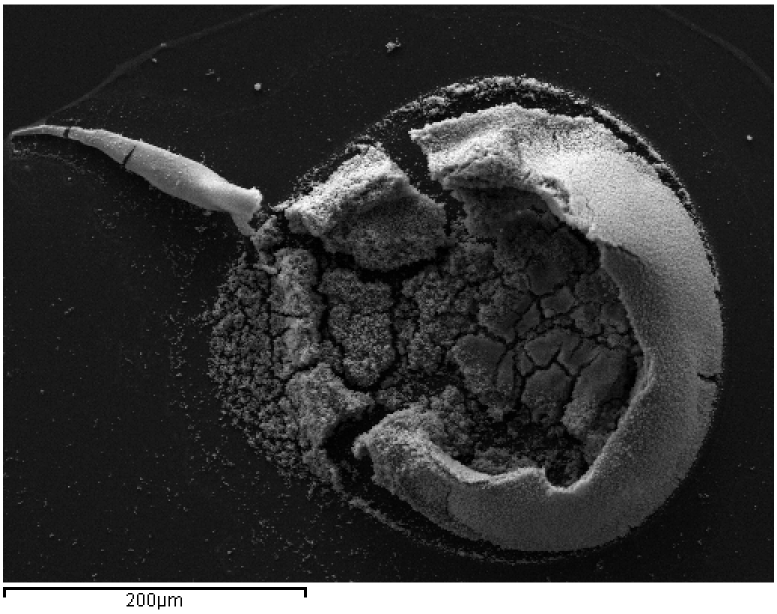

Figure S 25 – Higher magnification SEM image of the right hand membrane and tube.

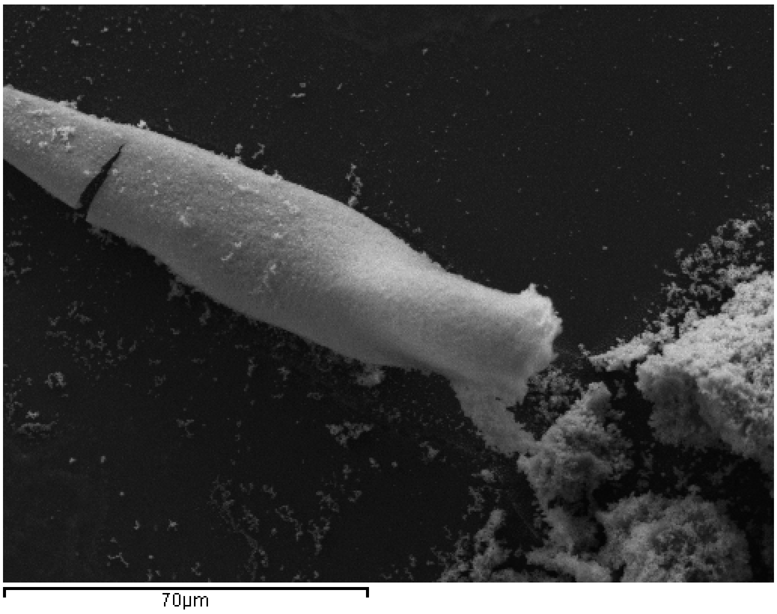

Figure S 26 – Higher magnification SEM image of the tube grown from the right hand membrane.

2 mM

These images show a pair of crystal which has formed a three dimensional semi-permeable membrane which has then burst to form a slug tube. The final image is of another sample in which microcrystallites are visible.

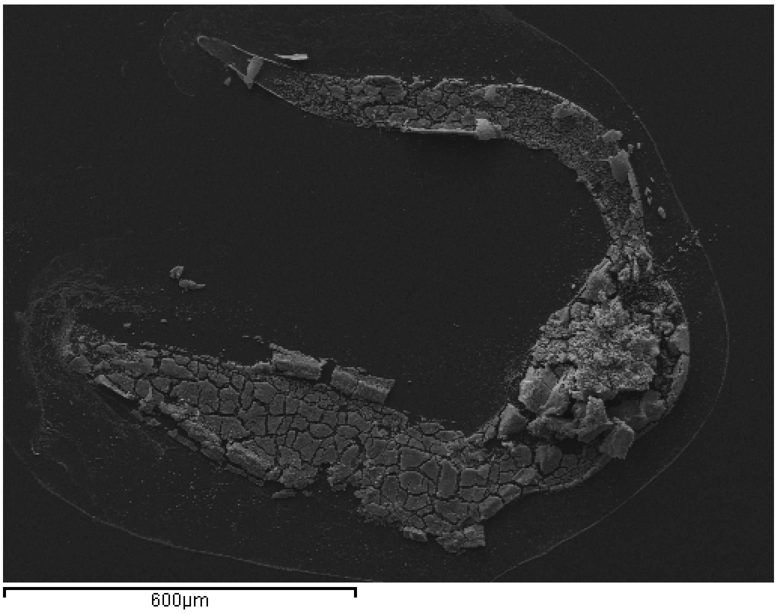

Figure S 27 – SEM image showing the membrane and slug tube formed on addition of 2 mM 2 to a crystal of 1.

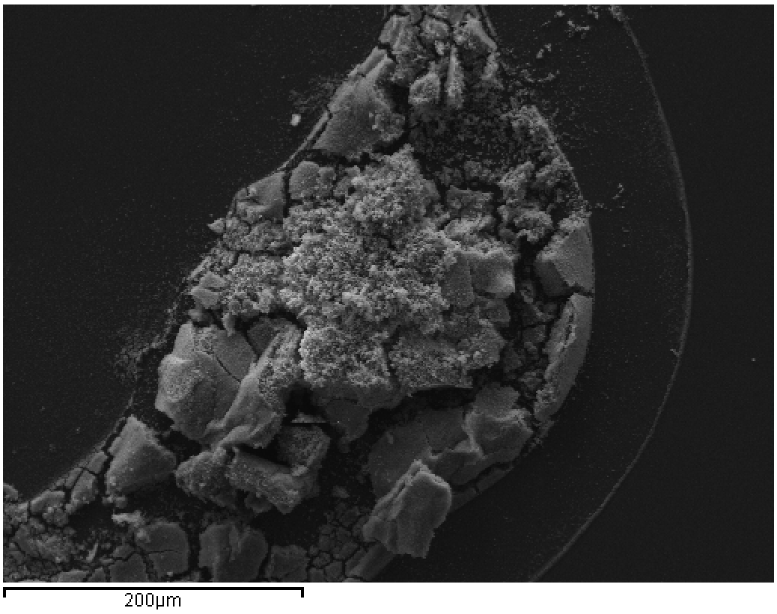

Figure S 28 - A higher magnification image of the membrane formed on addition of 2 mM 2 to a crystal of 1.

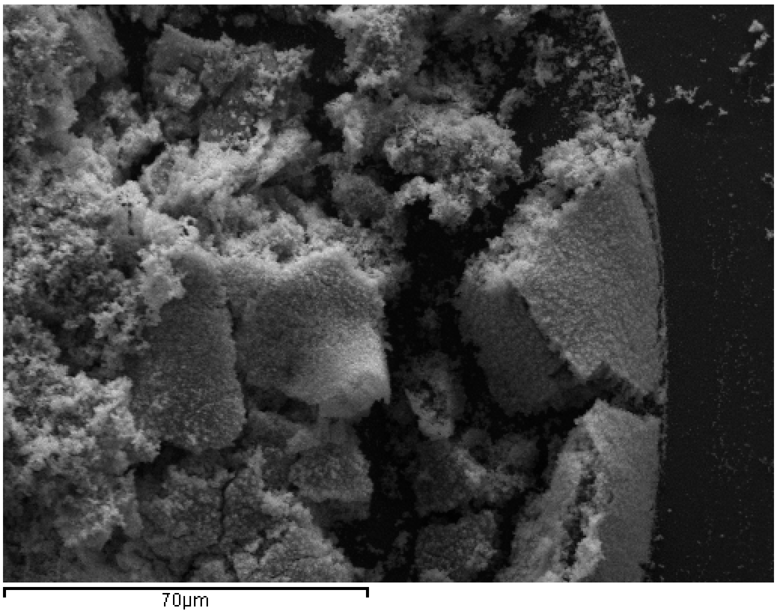

Figure S 29 - Figure S 15 - A higher magnification image of the membrane formed on addition of 2 mM 2 to a crystal of 1.

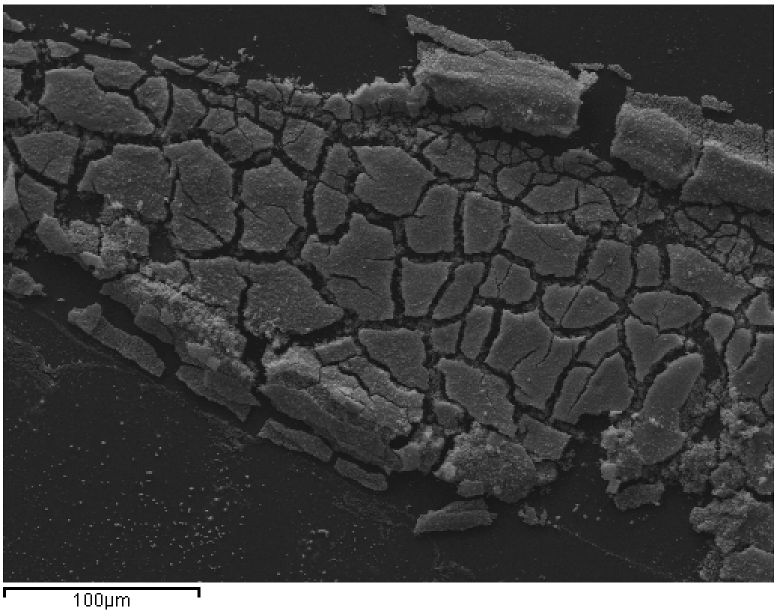

Figure S 30 - A higher mganification image showing the slug tube formed on addition of 2 mM 2 to a crystal of 1.

Figure S 31 – The overall precipitation structure formed on addition of 2 mM 2 to a crystal of 1. A slug tube can be seen, along with normal tubes.

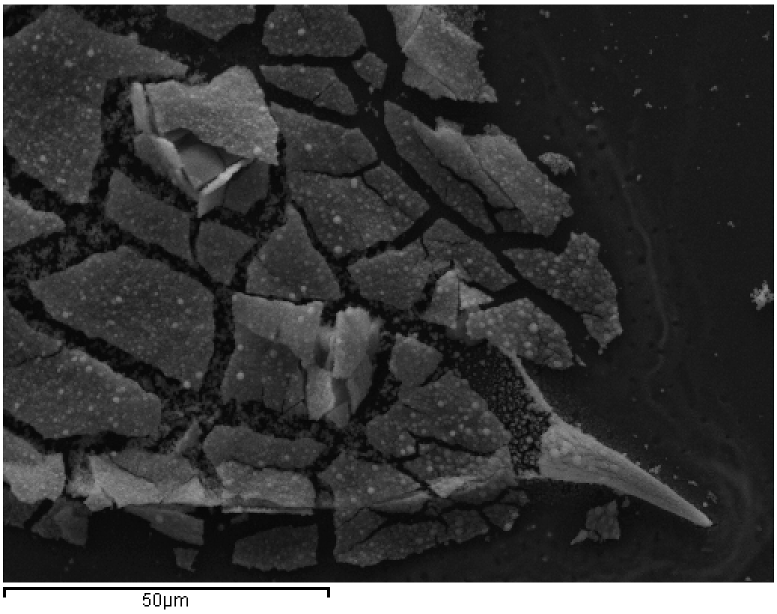

Figure S 32 – A higher magnification image of the end section of the precipitation structure formed on addition of 2 mM 2 to a crystal of 1. In this a short tube can be seen that grew after the main tube terminated along with microcrystallites that have grown within the tube.

5 mM

Figure S 33 - SEM image showing the tube and jetting precipitation structures formed when 5 mM 2 is added to a pair of crystals of 1.

Figure S 34 - SEM image showing the crystal and a tube formed when 5 mM 2 is added to a crystal of 1.

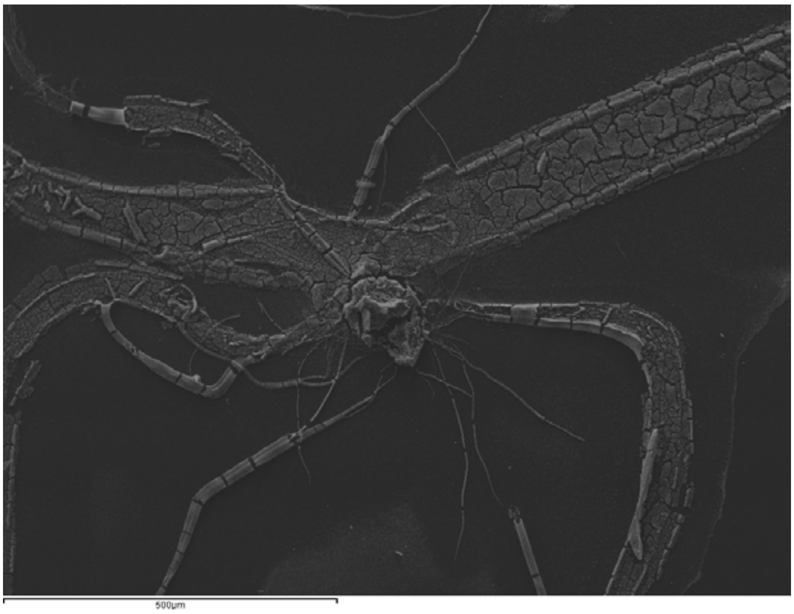

Figure S 35 - SEM image showing both tubes and jetting tubes formed from the same crystal on addition of 5 mM 2 to a crystal of 1.

Figure S 36 - SEM image showing both tubes and jetting tubes formed from the same crystal on addition of 5 mM 2 to a crystal of 1. Microcrystallites can also be seen growing .

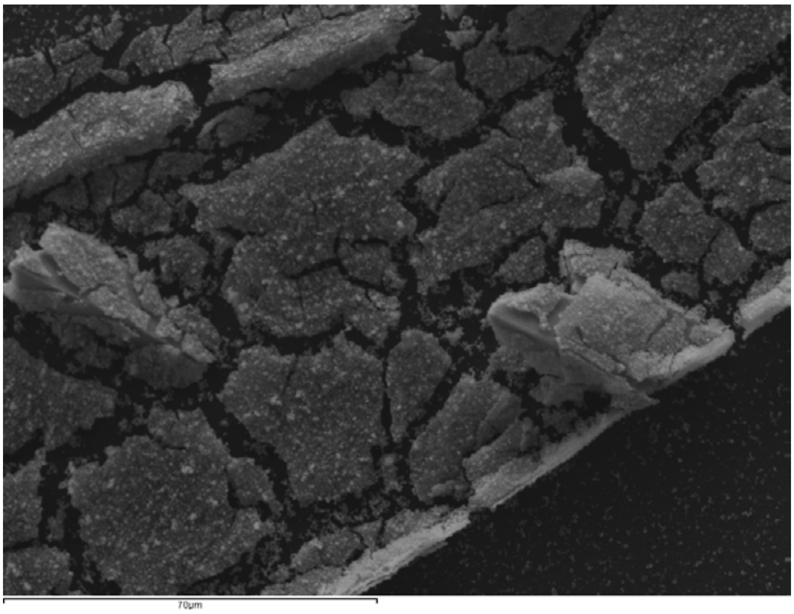

Figure S 37 - A higher magnification SEM image of the microcrystallites that formed inside the tube that grew on addition of 5 mM 2 to a crystal of 1.

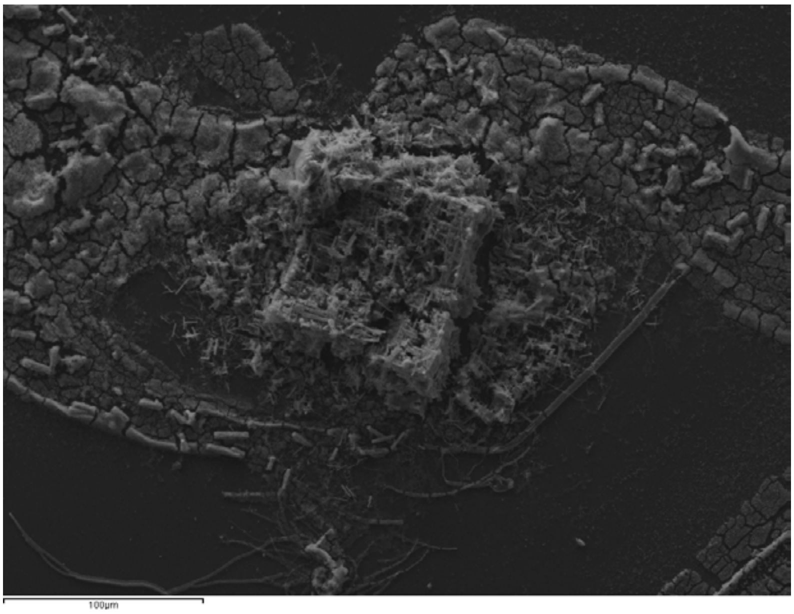

Figure S 38 - A higher magnification SEM image of the crystal seed after addition of 5 mM 2 to a crystal of 1, showing how seed material remains after precipitate structure has ceased.

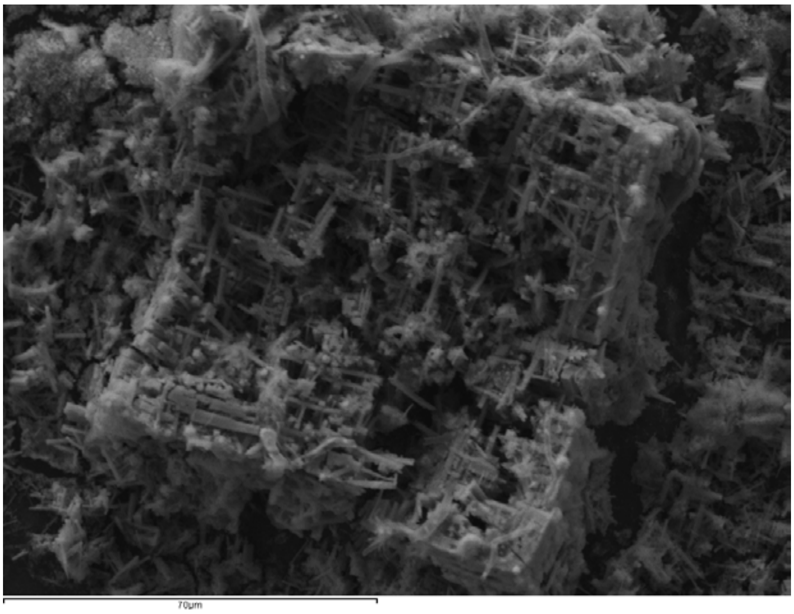

Figure S 39 - A higher magnification SEM image of the crystal seed after addition of 5 mM 2 to a crystal of 1, showing how seed material remains after precipitate structure has ceased.

10 mM

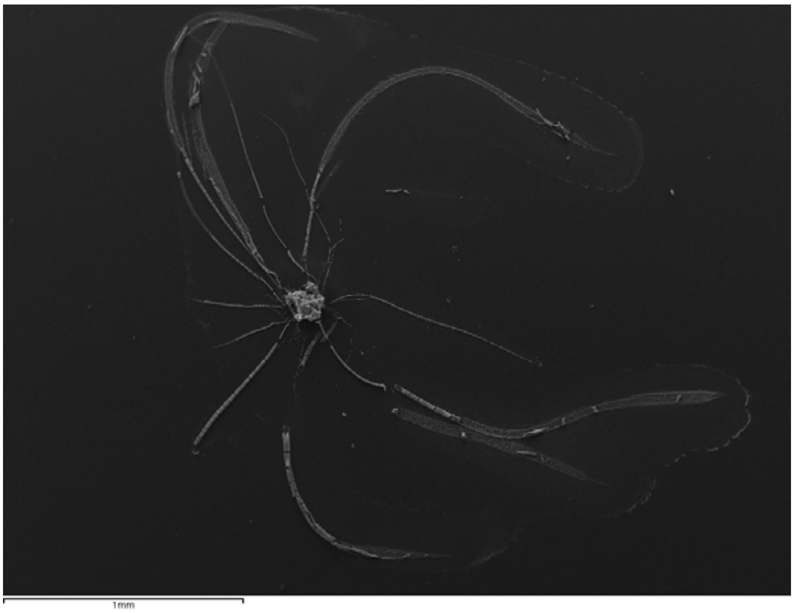

Figure S 40 - SEM image showing the jetting and tube precipitation structures formed when 10 mM 2 is added to a crystal of 1. The step changes in morphology that occur for some of the tubes are due to a tube growing off the surface coming into contact with, and subsequently growing along the surface.

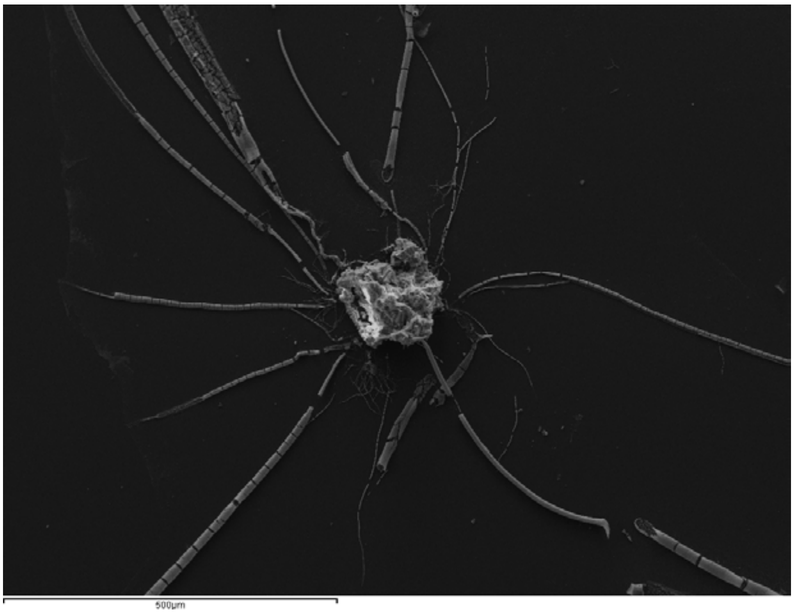

Figure S 41 - A higher magnification SEM image showing the area around the crystal after addition of 10 mM 2 to a crystal of 1.

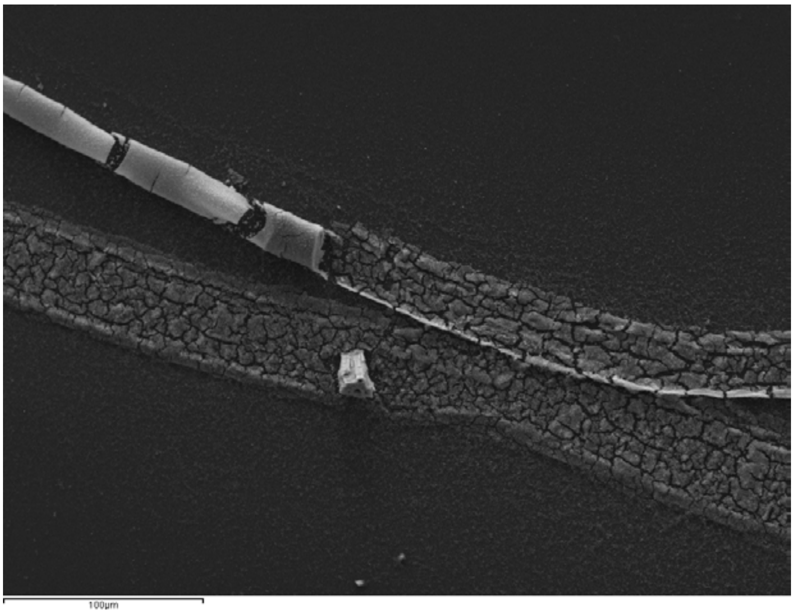

Figure S 42 - A higher magnification SEM image showing the point at which a tube comes into contact with the microscope slide after addition of 10 mM 2 to a crystal of 1. A tube can also be seen growing along the slide surface with a microcrystallite formed within it.

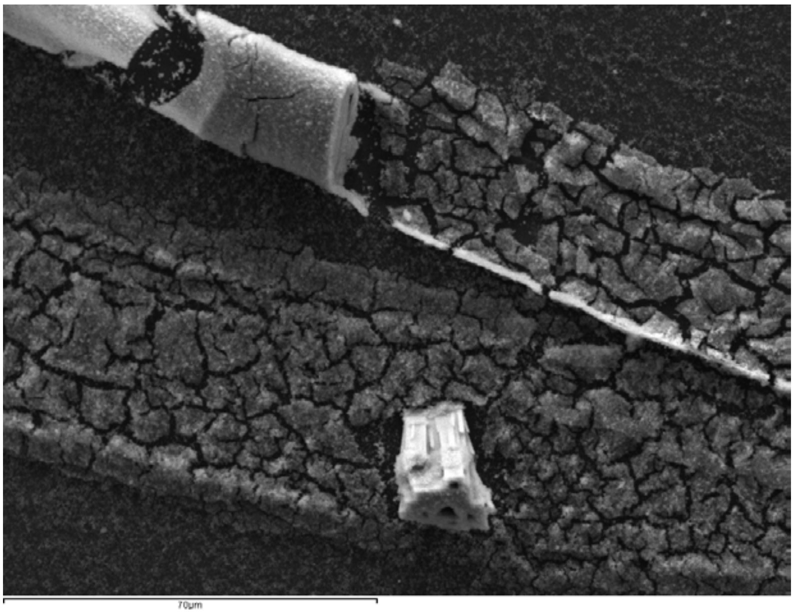

Figure S 43 – A higher magnification SEM image showing the point at which a tube comes into contact with the microscope slide after addition of 10 mM 2 to a crystal of 1. A tube can also be seen growing along the slide surface with a microcrystallite formed within it.

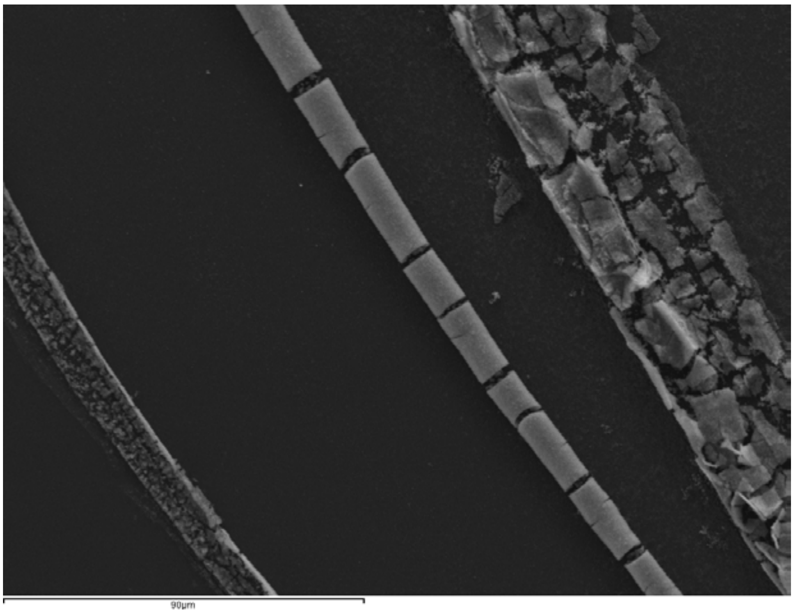

Figure S 44 - An SEM image illustrating the different surface morphologies observed for different tubes after addition of 10 mM 2 to a crystal of 1.

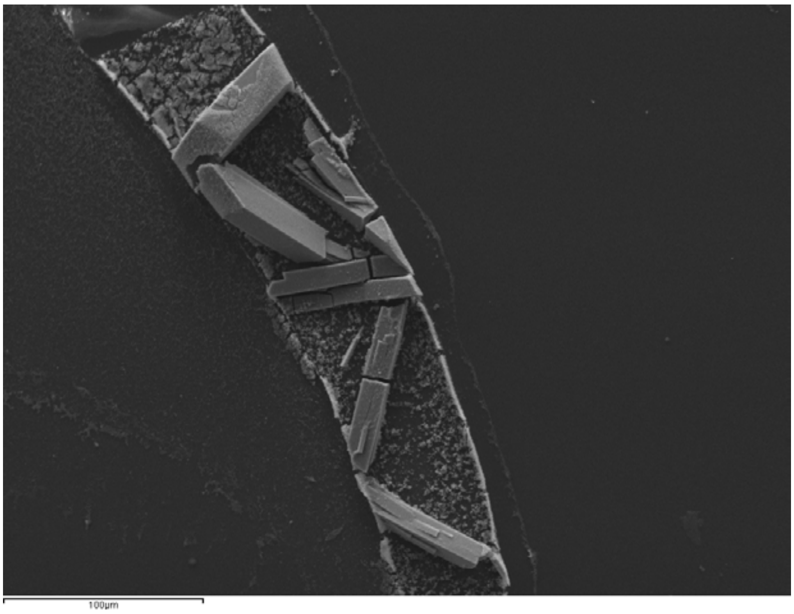

Figure S 45- An SEM image showing the microcrystallites that formed in a tube after addition of 10 mM 2 to a crystal of 1.

20 mM

At this concentration the thin jetting and budding tubes are very fragile and unfortunately a lot of them are washed away and broken during SEM sample preparation. As such, some of the thinnest tubes are not present in the SEM images, but both budding and jetting structures can be seen.

Figure S 46 - An SEM image of the overall precipitate structure formed from w crystal upon addition of 20 mM 2 to a crystal of 1.

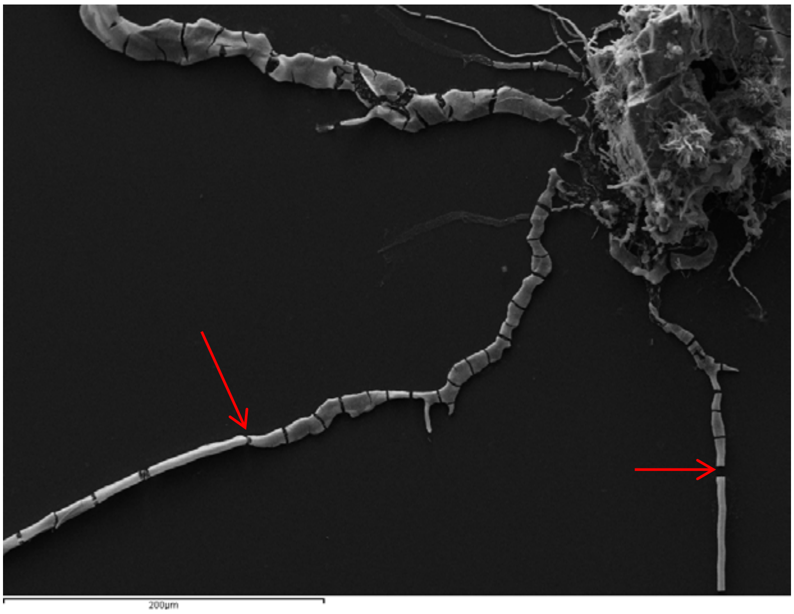

Figure S 47 – A higher magnification SEM image showing the crystal along with structures formed by both the budding and jetting growth regimes. The red arrows indicate roughly where the budding-jetting transition occurs, whilst the top tube forms due to budding for the whole length shown in this image. Also notice the small precipitation structures formed on the crystal surface.

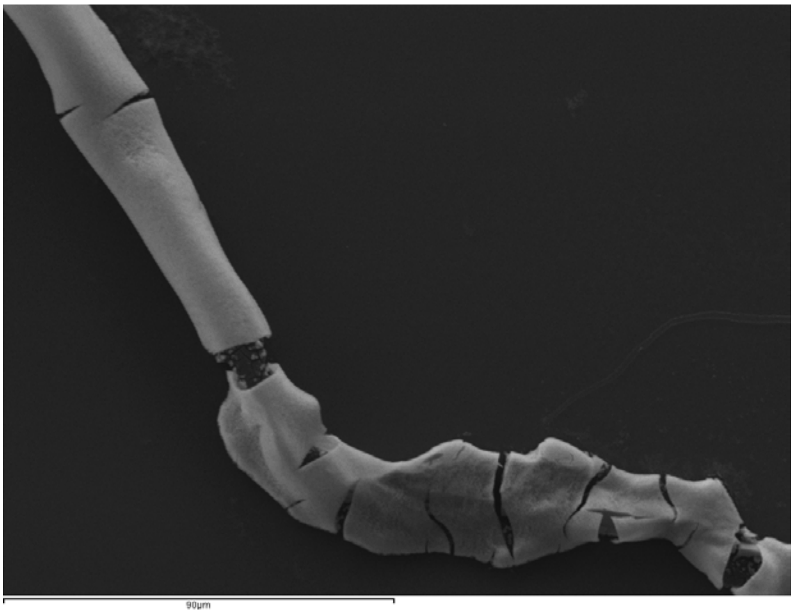

Figure S 48 - A higher magnification SEM image showing the transition point between the budding and jetting growth regimes. Notice how much smoother and straighter the tube is after it transitions to the jetting regime.

Figure S 49 – Another SEM image showing area of both the budding and jetting regimes as well as the precipitation structures on the crystal.

References

(1) Tézé, A.; Hervé, G. In *Inorganic Syntheses*; Klemperer, W. G., Ed.; 1990; Vol. 27, pp 88–92.

(2) Mialane, P.; Dolbecq, A.; Lisnard, L.; Mallard, A.; Marrot, J.; Sécheresse, F. *Angew. Chem. Int. Ed.* **2002**, *41* (13), 2398.